Dynamics of drop breakup in inhomogeneous turbulence at various volume fractions

SOPHIE GALINAT[1], FRÉDÉRIC RISSO[2]†, OLIVIER MASBERNAT[1] AND PASCAL GUIRAUD[3]

[1]Laboratoire de Génie Chimique, UMR 5503 CNRS-INP-UPS, 5 rue Paulin Talabot,
31106 Toulouse Cedex 1, France

[2]Institut de Mécanique des Fluides de Toulouse, UMR 5502 CNRS-INP-UPS,
Allée C. Soula, 31400 Toulouse, France

[3]Laboratoire d'Ingénierie des Procédés de l'Environnement, INSA Toulouse,
135 avenue de Rangueil, 31077 Toulouse Cedex 4, France

We report experimental and numerical determinations of the breakup probability of a drop travelling through inhomogeneous turbulent flow generated in a pipe downstream of a restriction. The model couples the Rayleigh–Lamb theory of drop oscillations with the Kolmogorov–Hinze theory of turbulent breakup. The interface deformation is modelled by a linear oscillator forced by the Lagrangian turbulent Weber number measured in experiments. The interface is assumed to rupture when either (i) the instantaneous Weber number exceeds a critical value or (ii) the predicted deformation exceeds a given threshold. Seven flow configurations have been tested, corresponding to various Reynolds numbers, damping coefficients and drop volume fractions. The history of the drop deformation proves to play an important role, and simulations assuming a critical Weber number fail to reproduce the experiments. Simulations assuming a critical deformation predict well the main features observed in the experiments. The linear oscillator appears able to describe the main feature of the dynamics of the drop deformation in inhomogeneous turbulence. Provided the oscillation frequency and the damping rate are known, the model can be used to compute the breakup probability in concentrated dispersed two-phase flows.

1. Introduction

The deformation of a drop (or bubble) in a turbulent flow combines two complex physical mechanisms: turbulence and interfacial-tension-driven flows. The purpose of this work is to determine the minimal description of these two mechanisms required to predict the occurrence of drop breakup. The first major step was achieved by Kolmogorov (1949) and Hinze (1955) who considered a drop immersed in isotropic turbulence, its diameter d being larger than the Kolmogorov microscale. The turbulence is accounted for only by the average turbulent stress $\overline{\tau}_t = \rho_c \overline{\delta u^2(d)}$, where ρ_c is the density of the continuous phase and $\overline{\delta u^2(d)}$ the mean square of the velocity difference over a distance d. The drop response is characterized by the restoring stress $\tau_i = \sigma/d$ generated by the surface tension σ. The breakup is assumed to occur when the average turbulent Weber number $\overline{We} = \overline{\tau}_t \tau_i^{-1}$ exceeds a critical

† Author to whom correspondence should be addressed: risso@imft.fr

value. The validity of this approach is limited since it ignores the temporal response of the interface to the unsteady turbulent forcing. The potential-flow Rayleigh–Lamb theory (Lamb 1932) however describes the drop dynamics as a series of oscillators, the principal mode of which is characterized by the frequency f_2,

$$f_2 = \frac{1}{2\pi} \sqrt{\frac{192\sigma}{(3\rho_d + 2\rho_c)d^3}}, \qquad (1.1)$$

and the damping rate β_2 (Miller & Scriven 1968),

$$\beta_2 = \frac{4(15\mu_d + 40\mu_c)}{(3\rho_d + 2\rho_c)d^2}, \qquad (1.2)$$

where ρ_d and μ_d (resp. ρ_c and μ_c) are the density and dynamic viscosity of the dispersed (resp. continuous) phase. Risso & Fabre (1998) showed that two different breakup regimes exist in turbulent flows. When the turbulent Weber number is large, the breakup results from the interaction of the drop with a single intense eddy. When the turbulent Weber number is small or moderate, individual turbulent eddies are not able to break the interface. However, if the residence time t_r of the drop in the turbulent flow is larger than the drop response time f_2^{-1}, interactions with several successive eddies may cause the breakup via stochastic resonance; the breakup probability then depends on t_r, f_2, β_2 and the turbulence time scales. Since the occurrence of breakup in a turbulent flow generally depends on the residence time, the breakup probability should be used instead of the critical Weber number (Risso 2000).

After the pioneering works by Ryskin & Leal (1984) and Kang & Leal (1989), several authors have performed numerical simulations of a drop in various basic flows in order to model its interaction with a single eddy: Shreekumar, Kumar & Gandhi (1996), Rodríguez-Rodríguez, Gordillo & Martínez-Bazán (2006), Revuelta, Rodríguez-Rodríguez & Martínez-Bazán (2006). The results of these simulations are related to real turbulent situations by the use of the Kolmogorov–Hinze scaling, which has been shown experimentally to correlate breakup statistics well when the Weber number is large (see Lasheras *et al.* 2002, and references therein). On the other hand, Kang & Leal (1990) have investigated the dynamics of a bubble in time-periodic straining flows by both the analysis of an approximate dynamic model and direct numerical simulations. To our knowledge, the only direct simulation considering a realistic turbulence was done by Qian *et al.* (2006) who computed the deformation of a drop in a homogeneous turbulence by using the lattice-Boltzmann method. Unfortunately, due to the high computational cost, the number of simulations, their duration and the domain size were drastically limited. At the present time, simpler models are probably more relevant for improving our understanding of the turbulent breakup.

O'Rourke & Amsden (1987) developed a model for drop breakup based on the forcing of shape oscillations by the turbulent flow. Known as the TAB model, it is commonly used in numerical simulations of sprays. Following a similar approach, Risso & Fabre (1998) computed the response of a single linear oscillator of frequency f_2 and damping rate β_2 forced by the instantaneous Weber number, $We(t) = \rho_c \delta u^2(t)d/\sigma$, measured in their experiment. The statistics of the deformation obtained from these computations were found to be in good agreement with the experimental results obtained with a bubble immersed in a homogeneous turbulent field under microgravity conditions. Whereas it is important to describe accurately the temporal evolution of the turbulence, a rather crude description of the interface seems to be sufficient to predict the statistics of the deformation. The objective of this work is

Phase	ρ (kg m^{-3})	μ (Pa s)	σ (N m^{-1})
Water	996	8.2×10^{-4}	23.6×10^{-3}
Water–glycerine	1100	4.7×10^{-3}	24.4×10^{-3}
Coloured heptane	683.7	4.5×10^{-4}	

TABLE 1. Properties of the liquids at 29°C: density, ρ; dynamic viscosity, μ; interfacial tension with coloured heptane, σ ($\sigma = 30.0 \times 10^{-3}$ N m^{-1} for pure heptane and water–glycerine).

to check whether this conclusion remains valid (i) when a drop travels through an inhomogeneous turbulent field and (ii) when it is surrounded by many other drops, as it is the case in most dispersed two-phase flows. Recently, the behaviour of liquid drops in the turbulent flow that develops downstream of an orifice in a pipe has been investigated experimentally (Galinat *et al.* 2005, 2007). Both the single-drop case and concentrated dispersed two-phase flows were investigated. They showed that the breakup probability depends on the drop location in the inhomogeneous turbulent field and cannot be accounted for by a single parameter, such as a global Weber number. In the present paper, these experimental results are revisited. The breakup probability is computed using model simulations similar to that of Risso & Fabre (1998) in order to determine if the time scale f_2 and β_2 are sufficient to describe the interface dynamics in situations (i) and (ii).

2. Experiments

The behaviour of a coloured drop of heptane has been investigated in four different carrier flows: single-phase flows of either water (A) or water–glycerine mixture (B) and dispersions of heptane drops in water–glycerine at volume fractions $\phi = 0.1$ (C) and $\phi = 0.2$ (D). The concentration of glycerine dissolved in water (43 % in mass) is adjusted to match the refractive indices of the two phases. In all case the two-phase mixture is thus transparent, only the coloured drop being visible. Table 1 reports the physical properties of the liquids. The experimental set-up and instrumentation are detailed in Galinat *et al.* (2005, 2007). The test section is a vertical pipe of internal diameter $D = 30$ mm with a concentric orifice of diameter $D_o = 15$ mm. The region under investigation extends from the orifice to 60 mm downstream. The velocity of the continuous phase is measured by means of high-speed PIV within a plane section passing through the pipe axis, with spatial and time resolutions of 0.55 mm and 0.5 ms. A high-speed camera is used to film the coloured drop at 500 frames s^{-1} (figure 1). The operating conditions are given in table 2. For the single-phase flow of water (A), the bulk velocity of the continuous phase through the orifice is $U_o = 0.60$ m s^{-1}, which corresponds to a Reynolds number $Re_o = \rho_c U_o D / \mu_c = 11 \times 10^3$. For the three other cases, two different bulk velocities have been investigated: $U_o = 0.60$ m s^{-1} and $Re_o = 2.1 \times 10^3$ (B1, C1, D1), $U_o = 0.90$ m s^{-1} and $Re_o = 3.1 \times 10^3$ (B2, C2, D2). For each flow configuration, coloured drops were injected individually upstream of the orifice; breakup was never observed before the drop had passed through the orifice. For the two-phase flows (C, D), an almost monodisperse and spatially homogeneous population of non-coloured heptane drops is also injected upstream of the orifice by means of an array of calibrated capillary tubes. The drop diameters are close to 2 mm, slightly changing with the flow rate.

Figure 2 shows the measured local average Weber number $\overline{We}$ for $U_o = 0.60$ m s^{-1} and $d = 2.4$ mm. The square of the velocity difference $\delta u^2(d)$ is calculated from the
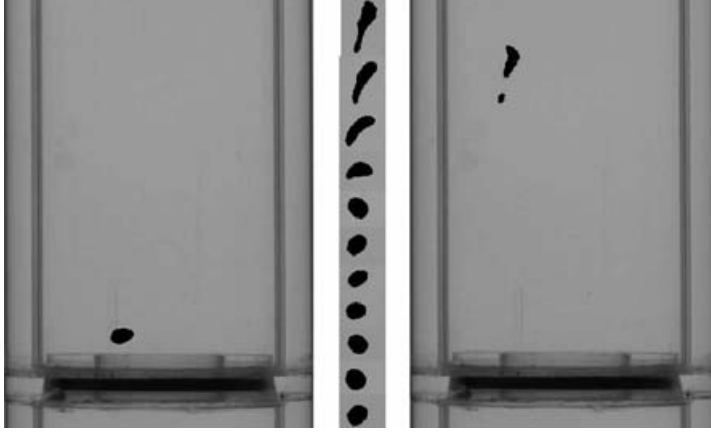
FIGURE 1. Drop shapes downstream of the orifice: near the orifice (left), intermediate shapes (middle), after the breakup (right).

Continuous phase case	Water A	Water–glycerine					
		B1	B2	C1	C2	D1	D2
ϕ	0	0	0	0.1	0.1	0.2	0.2
U_o (m s^{-1})	0.6	0.6	0.9	0.6	0.9	0.6	0.9
d_{exp}(mm)	2.5	2.2	2.3	1.8	1.8	2.0	1.9
d (mm)	2.4	2.4	2.4	1.9	1.9	1.9	1.9
ξ	0.024	0.113	0.113	0.127	0.127	0.127	0.127

TABLE 2. Operating conditions for experiments and numerical simulations: volume concentration of heptane drops, ϕ; bulk orifice velocity, U_o; average drop diameter in experiment, d_{exp}; drop diameter in simulations, d; damping coefficient, ξ.

instantaneous fluctuating velocity $\boldsymbol{u}(x, y)$, i.e. after subtraction of the mean velocity $\overline{U}(x, y)$ defined as the maximum of these of values in four directions (vertical x, transversal y and diagonals). In the radial direction there are strong mean-velocity gradients, but they do not generate pressure gradients and therefore do not contribute to the dynamic pressure $\rho_c \delta u^2(d)$. They might nevertheless cause drop deformations by generating a viscous stress, the amplitude of which is given by the capillary number, $Ca_U = \mu_c d \sigma^{-1} \partial \overline{U}_x / \partial y$. In the axial direction, the flow deceleration on the axis just downstream of the orifice also generates pressure variations that might deform the drop, with magnitude characterized by the Weber number $We_U = \rho_c d^3 \sigma^{-1} (\partial \overline{U}_x / \partial x)^2$. In all cases the deforming stresses induced by the mean flow are about two orders of magnitude smaller than that induced by the turbulent dynamic pressure. Turbulence is therefore the only cause of drop deformation for the drop diameters considered, which are much larger than the Kolmogorov microscale (a few tens micrometres) and slightly smaller than the turbulent integral length scale (about 3 mm).

Figure 2 shows that the regions of large turbulent intensities (i.e. large $\overline{We}$) of the three cases are different, indicating that the flow structure depends on both the Reynolds number and the drop volume fraction. We also observe that breakup locations (denoted by white crosses) coincide with the regions of large $\overline{We}$. For the single-phase flow of water (A), breakup occurs at the periphery of the jet that develops
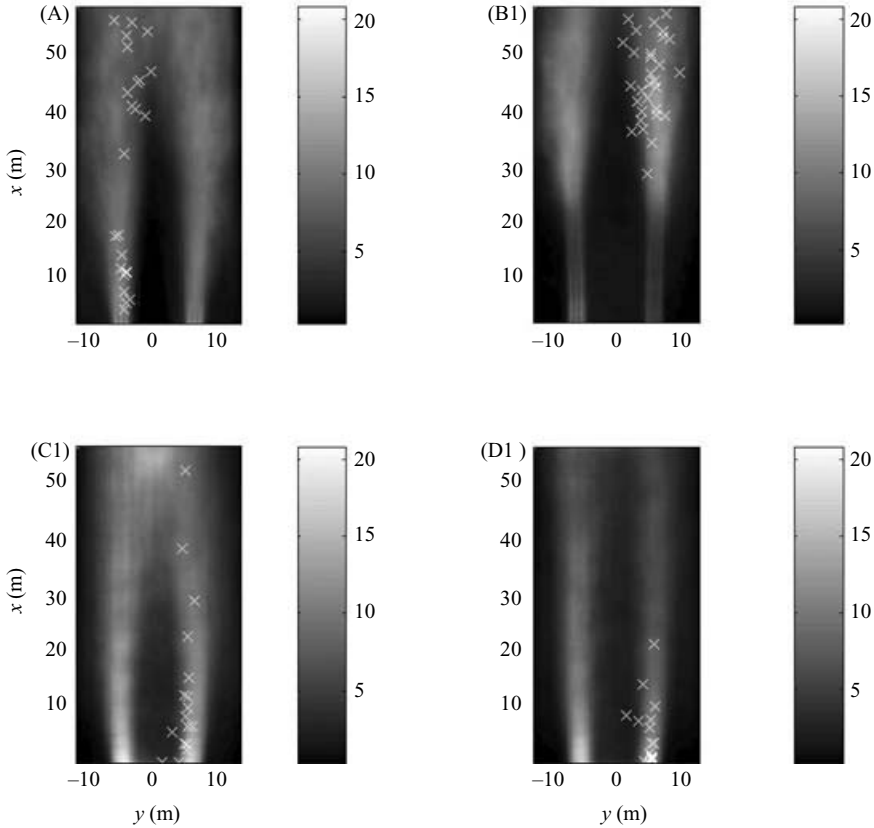
FIGURE 2. Measured average turbulent Weber number for $U_o = 0.6\,\mathrm{m\,s^{-1}}$: single-phase flow of water (A) and water–glycerine (B1); two-phase flows at $\phi = 0.1$ (C1) and $\phi = 0.2$ (D1). The symbols denote breakup locations.

just downstream of the orifice and also further downstream where the turbulence has diffused in the central region of the pipe. In case B1, no breakup is observed close to the orifice. In two-phase flow case at $\phi = 0.1$ (C1), breakup events are distributed all along the pipe, whereas at $\phi = 0.2$ (D1), they are concentrated close to the orifice.

3. Modeling and simulations of drop dynamics

Experimental results have shown a strong relationship between the local structure of the turbulence and breakup occurrences. We now determine the role of the interface dynamics. Our approach consists of computing the behaviour of a drop in the instantaneous velocity field of the continuous phase, $U(x, y, t)$.

The drop centre is initially located 2 mm downstream of the orifice and its radial position is randomly chosen in the range $[-(D_o - d)/2, (D_o - d)/2]$ by assuming a uniform probability per unit of area of the orifice. The time evolution of the drop position $x(t)$ is then calculated by assuming that the drop velocity is the sum of the continuous-phase velocity plus a constant vertical drift velocity $U_d\,e_x$:

$$\frac{\mathrm{d}x(t)}{\mathrm{d}t} = U(x, y, t) + U_d\,e_x, \tag{3.1}$$

where e_x is the unit vector opposite to gravity. Equation (3.1) is solved by using experimental records of the velocity $U(x, y, t)$. Since U is only measured in a vertical

axial plane, we will assume that the drop trajectory is two-dimensional. The drift velocity is calculated from experimental correlations of Augier, Masbernat & Guiraud (2003): in single-phase flow, U_d is assumed to be the terminal rise velocity V_t of a drop rising in a fluid at rest; in two-phase flow, the effect of the drop volume fraction is accounted for by $U_d = V_t \exp(-4.6\phi)$.

In all cases, the drift velocity U_d is less than $\frac{1}{5}U_o$ and the drop motion is dominated by the continuous phase velocity. We checked that the computed motion was in agreement with the experiments: trajectories are similar and the average and standard deviation of the drop velocity against the axial position are reproduced well. Note that the combination of (3.1) with the correlations of Augier *et al.* (2003) does not constitute a general model valid for other flow configurations: the important point here is that it predicts well the drop residence time in each region of the present flow.

The deformation of the interface is characterized by the amplitude A_2 of the second spherical harmonic, which is the dominant eigenmode of the linear Rayleigh–Lamb theory. It involves a periodic succession of lengthening and flattening at frequency f_2 and damping rate β_2 (see Risso 2000). The turbulence force responsible for drop deformation is assumed to be proportional to the product of the instantaneous Kolmogorov–Hinze stress τ_t and the drop area. The mass of fluid set in motion by the drop oscillation is propotionnal to $\sigma/(4\pi^2 f_2^2) = (3\rho_d + 2\rho_c)d^3/192$ and the interface dynamics described by

$$\frac{\sigma}{\left(4\pi^2 f_2^2\right)} \frac{\mathrm{d}^2 A_2}{\mathrm{d}t^2} + \frac{2\beta_2\sigma}{\left(4\pi^2 f_2^2\right)} \frac{\mathrm{d}A_2}{\mathrm{d}t} + \sigma A_2 = K\rho_c\delta u^2(d, x, y, t)d^2. \tag{3.2}$$

After normalizing the amplitude A_2 by d, the time t by $1/(2\pi f_2)$ and marking the dimensionless quantities with a tilde, (3.2) becomes

$$\frac{\mathrm{d}^2 \tilde{A}_2}{d\tilde{t}^2} + 2\xi \frac{\mathrm{d}\tilde{A}_2}{\mathrm{d}\tilde{t}} + \tilde{A}_2 = K\frac{\rho_c\delta u^2 d}{\sigma} = K\,We(d, x, y, \tilde{t}), \tag{3.3}$$

where $\xi = \beta_2/(2\pi f_2)$ is the damping coefficient and $We(d, x, y, \tilde{t})$ is the instantaneous turbulent Weber number at instant $\tilde{t}$ obtained from the PIV record at the drop location $x(\tilde{t})$. The system (3.1), (3.3) is solved numerically by using a first-order scheme with a time step $\delta\tilde{t} = 2\pi \times 10^{-3}$ and for a computational time $6\pi \leqslant \tilde{t} \leqslant 14\pi$, allowing the drop to cross the measuring section. In agreement with experimental observations the drop is initially assumed to be spherical ($\tilde{A}_2 = 0$). We did not find any theoretical approaches for determining the value of the prefactor K which arises from the matching of the Rayleigh–Lamb theory with that of Kolmogorov–Hinze. However, since (3.3) is linear, the simulations have been done with K set to unity without lost of generality; this simply means that we computed $\tilde{A}_2/K$ instead of $\tilde{A}_2$. The values of f_2 and β_2 have been calculated by inserting the experimental physical properties into the theoretical expressions (1.1) and (1.2). The damping coefficient ξ is given in table 2; that for water–glycerine is about twice that for water.

Two different breakup criteria have been tested. The first postulates that the drop ruptures when the instantaneous Weber number exceeds a critical value: $We(\tilde{t}) > We_c$. This criterion accounts for the inhomogeneous character of the turbulence but ignores the time response of the interface to the turbulent forcing. In this case, the instantaneous deformation is considered to be proportional to the instantaneous Weber number. The second criterion postulates that breakup occurs when the deformation exceeds a critical value: $\tilde{A}_2(\tilde{t}) > \tilde{A}_{2c}$. In both cases, the critical value, We_c or $\tilde{A}_{2c}/K$, is the only adjustable parameter.

Figure 3 presents two examples of computed deformation corresponding to the single-phase flow of water (A) and water–glycerine (B1) at $U_o = 0.60\,\mathrm{m\,s}^{-1}$. The
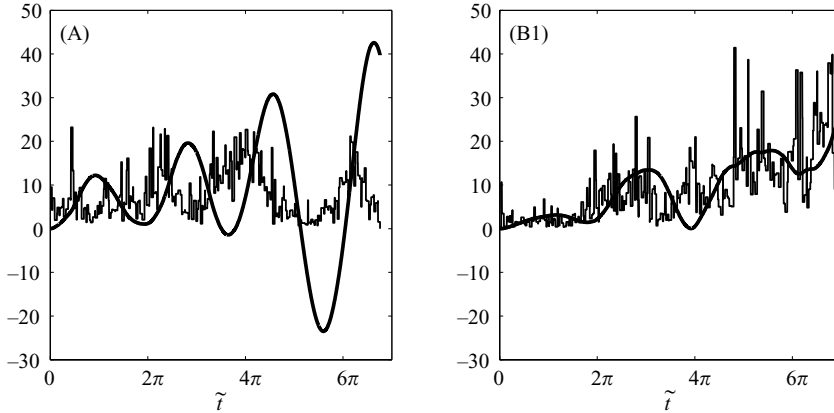
FIGURE 3. Numerical simulations of single-phase flow at $U_o = 0.6\,\mathrm{m\,s^{-1}}$: (A) water, (B1) water–glycerine. Thin lines: $We(t)$; thick lines $\tilde{A}_2(\tilde{t})/K$.

experimental signal $We(\tilde{t})$ contains frequencies much higher than $\tilde{f}_2 = 1/(2\pi)$. Since these frequencies are filtered by the dynamical system (3.3), $\tilde{A}_2(\tilde{t})$ is smoother and exhibits dominant oscillations at frequency $\tilde{f}_2$. These two examples show that the drop deformation may evolve differently than the Weber number. In case A, $\tilde{A}_2(\tilde{t})$ regularly increases due to stochastic resonance whereas $We(\tilde{t})$ fluctuates around a constant mean value. In case B1, $\tilde{A}_2(\tilde{t})$ cannot follow the large variations of $We(\tilde{t})$. Two hundred numerical simulations have been carried out for each experimental configuration. Denoting the axial position of a drop relative to the orifice as x, we defined the probability $F(X)$ that a drop splits off while x belongs to the interval $[0,X]$. $F(X)$ starts from zero at $X = 0$ and then characterizes the increase of the breakup probability with the distance from the orifice. It has been calculated for each flow configuration and breakup criterion. From these two examples, we anticipate that the two breakup criteria will lead to significantly different results.

4. Results and discussion

We now compare the computed and experimental breakup probabilities to determine whether the present model can deal with the various flow configurations investigated, characterized by different Reynolds numbers, damping rates and drop volume fractions.

Let us consider first single-phase flow cases. Thick lines in figure 4 show the experimental breakup probability for water (A) and water–glycerine (B1) flows at $U_o = 0.6\,\mathrm{m\,s^{-1}}$. The two situations are very different since in water ($Re_o = 11 \times 10^3$) the probability starts increasing just beyond the orifice, whereas in water–glycerine ($Re_o = 2.1 \times 10^3$) it remains null up to $x = 3\,\mathrm{cm}$. Thin lines in figure 4 represent the breakup probability computed with the criterion based on a critical Weber number for $We_c = 30$, 35 and 40. In water (A), the evolution of $F(X)$ is reasonably well reproduced for $We_c = 20$. However, in water–glycerine (B1), the simulations fail to predict the absence of breakup in the region close to the orifice. Therefore, although the location of breakup events is observed to coincide with the regions of large $\overline{We}$ (figure 2), breakup occurrence does not depend only on the instantaneous value of We.

Thick lines in figure 5 again show the experimental breakup probability for single-phase flow of water at $U_o = 0.6\,\mathrm{m\,s^{-1}}$ (A) and water–glycerine at $U_o = 0.6\,\mathrm{m\,s^{-1}}$ (B1)
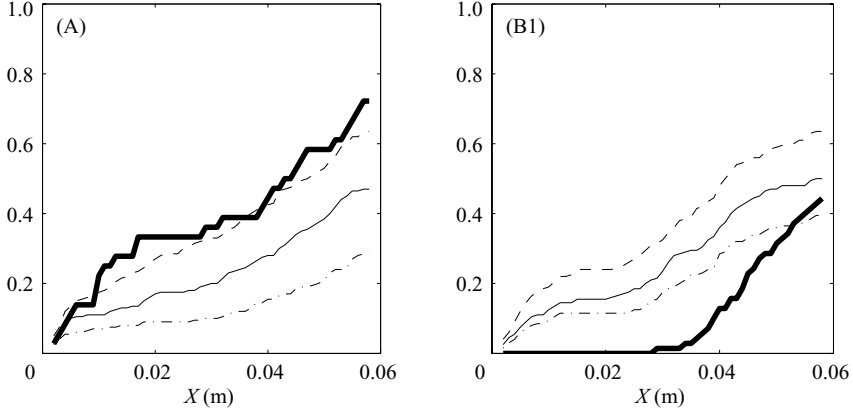
FIGURE 4. Breakup probability $F(X)$ in single-phase flow at $U_o = 0.6\,\mathrm{m\,s^{-1}}$: (A) water; (B1) water–glycerine. Thick lines: experiments. Thin lines: numerical simulations assuming a critical Weber number, $We_c = 30$ (dashed line), 35 (solid line) or 40 (dot-dashed line).
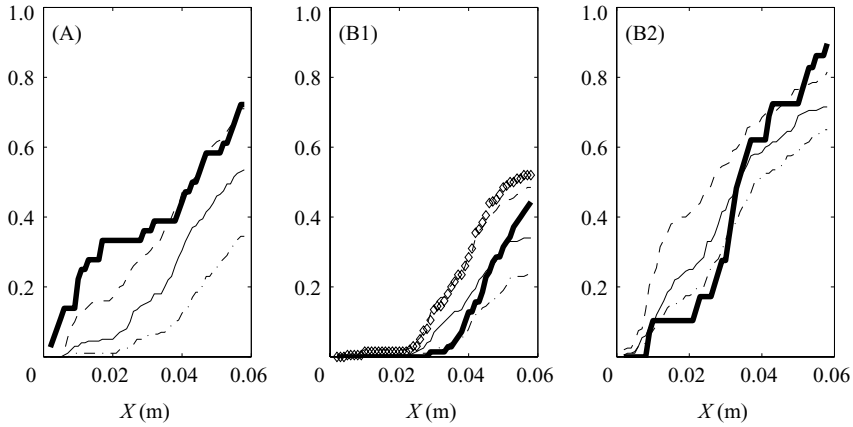.

FIGURE 5. Breakup probability, $F(X)$, in single-phase flow: (A) water and (B1) water–glycerine at $U_o = 0.6\,\mathrm{m\,s^{-1}}$; (B2) water–glycerine at $U_o = 0.9\,\mathrm{m\,s^{-1}}$. Thick lines: experiments. Thin lines: numerical simulations assuming a critical deformation, $\tilde{A}_{2c}/K = 20$ (dashed line), 25 (solid line) or 30 (dot-dashed line). Symbols: numerical simulation for $\tilde{A}_{2c}/K = 25$ with a smaller damping, $\xi = 0.024$.

and at $U_o = 0.9\,\mathrm{m\,s^{-1}}$ (B2). Thin lines now represent the breakup probability computed by assuming a criterion based on the instantaneous deformation, for $\tilde{A}_{2c}/K = 20$, 25 and 30. In case A the breakup probability predicted with this criterion is quite similar to that obtained with the Weber criterion, and is close to the experimental one for $\tilde{A}_{2c}/K = 20$. On the other hand, in case B1, the results obtained with the amplitude criterion are much better: the absence of breakup close to the orifice is now reproduced well, the best agreement with the experimental results being obtained for $\tilde{A}_{2c}/K$ close to 25. With the same value of $\tilde{A}_{2c}/K$, the model also reproduces well the very different evolution of $F(X)$ observed at a larger velocity in water–glycerine (B2). The description of the drop dynamics by the forced linear oscillator (3.3) together with the breakup criterion based on a critical deformation is hence sufficient to predict the different evolutions of the breakup probability observed in the present configurations.
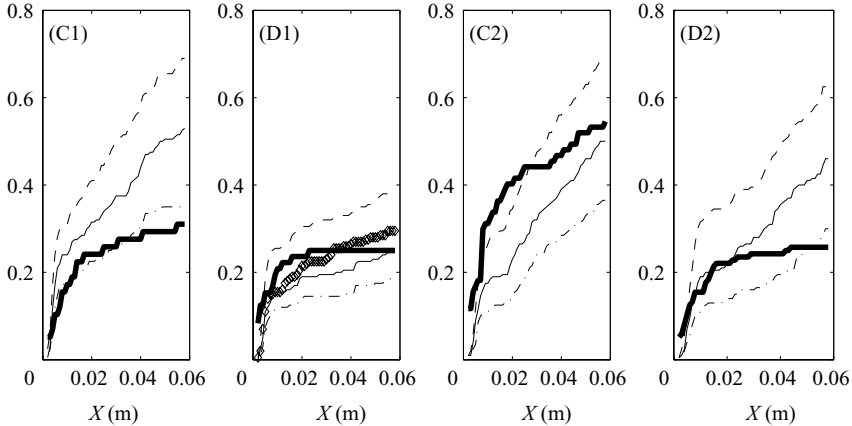
FIGURE 6. Breakup probability, $F(X)$, in two-phase flow: $\phi = 0.1$ (C1) and $\phi = 0.2$ (D1) for $U_o = 0.6\,\mathrm{m\,s^{-1}}$; $\phi = 0.1$ (C2) and $\phi = 0.2$ (D2) for $U_o = 0.9\,\mathrm{m\,s^{-1}}$. Thick lines: experiments. Thin lines: numerical simulations assuming a critical deformation, $\tilde{A}_{2c}/K = 25$ (dashed line), 30 (solid line) or 35 (dot-dashed line). Symbols: simulation for $\tilde{A}_{2c}/K = 25$ with a larger damping rate, $\xi = 0.16$.

Note that between cases A ($Re_o = 2.1 \times 10^3$, $\xi = 0.024$) and B1 ($Re_o = 2.1 \times 10^3$, $\xi = 0.113$), both the flow structure and the damping coefficient have been changed. To disentangle their effects, we have computed the breakup probability of case B1 by taking the value of the damping coefficient corresponding to case A. The corresponding result for $\tilde{A}_{2c}/K = 25$ is represented by the symbols in figure 5. Decreasing the damping coefficient from 0.113 to 0.024 increases the breakup probability, changing the curve obtained for $\tilde{A}_{2c}/K = 25$ into approximately that obtained for $\tilde{A}_{2c}/K = 20$. Even though the deformation is driven by inertia, viscosity influences the breakup probability by fixing the damping rate of drop oscillations. However it is worth noting that the effect of the damping rate is not enough strong to change the behaviour of case B1 into that of case A.

We now address concentrated two-phase flows, in which the test drop is surrounded by many other drops that may influence its dynamics. Figure 6 shows the breakup probability for two drop volume fractions ($\phi = 0.1$ and 0.2) and two flow velocities ($U_o = 0.6$ and $0.9\,\mathrm{m\,s^{-1}}$). In all cases the experimental breakup probability (thick line) is reasonably well reproduced by the simulations (thin line) assuming a critical amplitude $\tilde{A}_{2c}/K$ between 25 and 35. Although the differences in the flow structure between the four cases have been accounted for by using the corresponding measured $We(t)$, the theoretical expressions (1.1), (1.2) used for calculating the oscillation frequency and damping rate do not include the possible effect of drop interactions. In the absence of any available theory, we have performed additional simulations with various values of the damping rate. Symbols in figure 6 represent the probability computed for case D1 ($\phi = 0.2$, $U_o = 0.6\,\mathrm{m\,s^{-1}}$) by using $\xi = 0.16$ (instead of $\xi = 0.127$). With this particular value of ξ, the computed probability matches the experiments for the same critical amplitude as in single-phase flow ($\tilde{A}_{2c}/K = 25$).

Risso & Fabre (1998) showed that the model (3.3) which couples Rayleigh–Lamb theory of drop oscillation with the Kolmogorov–Hinze theory of turbulent breakup contains the main physics of the interface deformation for a bubble in a homogeneous turbulent field. The present results extend its validity to the case of a drop travelling through an inhomogeneous turbulent field and to that of concentrated drop dispersions. Assuming that breakup occurs for a given deformation is therefore in

agreement with the experiments of Risso & Fabre (1998) and the present observations. Here, the drop length at breakup is about twice the initial diameter ($\tilde{A}_{2c} \approx 1$), which implies that the prefactor K in (3.3) should be set to about $1/25$ for the computed amplitude A_2 to represent the maximal drop extension. Investigations of other configurations are required to determine whether K may depend on the structure of the turbulent flow and on the deformation time scales. For concentrated dispersions, theoretical expressions for f_2 and β_2 accounting for drop interactions are also needed.

REFERENCES

AUGIER, F., MASBERNAT, O. & GUIRAUD, P. 2003 Slip velocity and drag law in a liquid-liquid homogeneous dispersed flow. *AIChE J.* **49**, 2300–2316.

GALINAT, S., GARRIDO TORRES, L., MASBERNAT, O., GUIRAUD, P., RISSO, F., DALMAZZONE, C. & NOÏK, C. 2007 Break-up of a drop in a liquid-liquid pipe flow through an orifice. *AIChE J.* **53** (1), 56–68.

GALINAT, S., MASBERNAT, O., GUIRAUD, P., DALMAZZONE, C. & NOÏK, C. 2005 Drop break-up in turbulent pipe flow downstream of a restriction. *Chem. Engng Sci.* **60**, 6511–6258.

HINZE, J. O. 1955 Fundamentals of the hydrodynamic mechanism of splitting in dispersion processes. *AIChE J.* **1**, 289–295.

KANG, I. S. & LEAL, L. G. 1989 Numerical solution of axisymmetric, unsteady free-boundary problems at finite Reynolds number. II. Deformation of a bubble in a biaxial straining flow. *Phys. Fluids* A **1**, 644–660.

KANG, I. S. & LEAL, L. G. 1990 Bubble dynamics in time-periodic straining flows. *J. Fluid Mech.* **218**, 41–69.

KOLMOGOROV, A. N. 1949 On the disintegration of drops in a turbulent flow. *Dokl. Akad. Nauk. SSSR* **66**, 825–828.

LAMB, H. 1932 *Hydrodynamics.* Cambridge University Press.

LASHERAS, J. C., EASTWOOD, C., MARTÍNEZ-BAZÁN, C. & MONTAÑÉS, J. L. 2002 A review of statistical models for the break-up of an immiscible fluid immersed into a fully developed turbulent flow. *Intl J. Multiphase Flow* **28**, 247–278.

MILLER, C. A. & SCRIVEN, L. E. 1968 The oscillations of a fluid droplet immersed in another fluid. *J. Fluid Mech.* **32**, 417–435.

O'ROURKE, P. J. & AMSDEN, A. A. 1987 The TAB method for numerical calculation of spray droplet breakup. *SAE Technical Paper* 872089.

QIAN, D., MACLAUGHLIN, J. B., SANKARANARAYANAN, K., SUNDARESAN, S. & KONTOMARIS, K. 2006 Simulation of bubble breakup dynamics in homogeneous turbulence. *Chem. Engng Commun.* **193**, 1038–1063.

REVUELTA, A., RODRÍGUEZ-RODRÍGUEZ, J. & MARTÍNEZ-BAZÁN, C. 2006 Bubble break-up in a straining flow at finite Reynolds numbers. *J. Fluid Mech.* **551**, 175–184.

RISSO, F. 2000 The mechanisms of deformation and breakup of drops and bubbles. *Multiphase Sci. Tech.* **12**, 1–50.

RISSO, F. & FABRE, J. 1998 Oscillations and breakup of a bubble immersed in a turbulent field. *J. Fluid Mech.* **372**, 323–355.

RODRÍGUEZ-RODRÍGUEZ, J., GORDILLO, J. M. & MARTÍNEZ-BAZÁN, C. 2006 Breakup time and morphology of drops and bubbles in a high-Reynolds-number flow. *J. Fluid Mech.* **548**, 69–86.

RYSKIN, G. & LEAL, L. G 1984 Numerical solution of free-boundary problems in fluid mechanics. Part 3. Bubble deformation in an axisymmetric straining flow. *J. Fluid Mech.* **148**, 37–43.

SHREEKUMAR, KUMAR, R. & GANDHI, K. S. 1996 Breakage of a drop of inviscid fluid due to a pressure fluctuation at its surface. *J. Fluid Mech.* **328**, 1–17.